SCIENTIFIC REPORTS

OPEN

SUBJECT AREAS:
MATERIALS FOR ENERGY AND CATALYSIS
MATERIALS SCIENCE

Received
10 October 2013

Accepted
19 November 2013

Published
9 December 2013

Correspondence and requests for materials should be addressed to N.W. (wangninguestc@gmail.com) or K.K. (g44233@nucc.cc.nagoya-u.ac.jp)

Enhanced thermoelectric performance of Nb-doped $SrTiO_3$ by nano-inclusion with low thermal conductivity

Ning Wang[1], Haijun Chen[1], Hongcai He[1], Wataru Norimatsu[2], Michiko Kusunoki[2] & Kunihito Koumoto[2]

[1]University of Electronic Science and Technology of China, State Key Laboratory of Electronic Thin Films and Integrated Devices, Chengdu, 610054, P. R. China, [2]Nagoya University, Graduate School of Engineering, Nagoya, 464-8603, Japan.

Authors reported an effective path to increase the electrical conductivity while to decrease the thermal conductivity, and thus to enhance the *ZT* value by nano-inclusions. By this method, the *ZT* value of Nb-doped $SrTiO_3$ was enhanced 9-fold by yttria stabilized zirconia (YSZ) nano-inclusions. YSZ inclusions, located inside grain and in triple junction, can reduce the thermal conductivity by effective interface phonon scattering, enhance the electrical conductivity by promoting the abnormal grain growth, and thus lead to the obvious enhancement of *ZT* value, which strongly suggests that, it is possible to not only reduce the thermal conductivity, but also increase the electrical conductivity by nano-inclusions with low thermal conductivity. This study will give some useful enlightenment to the preparation of high-performance oxide thermoelectric materials.

Thermoelectric (TE) energy conversion is a promising technology for both electricity power generation in harvesting wasted heat and electric cooling. The efficiency of TE devices is characterized by the dimensionless figure of merit, $ZT = (S^2\sigma/\kappa)T$, where S, σ, κ, and T are the Seebeck coefficient, the electrical conductivity, the thermal conductivity, and the absolute temperature, respectively. To date, most of the discovered bulk materials with high *ZT* values exhibit thermal and chemical instability in air, and are composed of toxic, scarce or expensive elements[1–5]. Recently, various ceramic oxide thermoelectric (TE) materials have attracted widespread attention, because they are economical, environmentally-friendly, possess various chemical compositions, and consist of naturally abundant[6–14]. So far, among the *p*-type oxide thermoelectric bulk materials, the textured BiCuSeO has the highest *ZT* value, ~1.4 at 923 K[15], which can meat the basic requirements of practical applications. Both *p*-type and *n*-type oxide materials are needed to construct an efficient thermoelectric device. However, among the *n*-type oxide thermoelectric bulk materials, even though Nb-doped $SrTiO_3$ bulk ceramic has the highest *ZT* value so far[16], but it is still very low, compared with *p*-type textured BiCuSeO, and thus urgently needs to improve.

In 2007, Dresselhaus *et al.* proposed that nanocomposite thermoelectric materials would offer a promising approach for the preparation of bulk samples with nano-sized constituents[17]. Since then, a variety of nanocomposites with higher thermoelectric properties than bulk materials have been prepared. Tang *et al.* prepared Bi_2Te_3 bulk materials with layered nanostructure by combining melt spinning technique with spark plasma sintering, and the maximum *ZT* value of 1.35 was obtained at 300 K[18]. Mi *et al.* prepared *n*-type $CoSb_3$ nanocomposites by hot pressing the mixture of nanoscale and microsized $CoSb_3$ powders, and the maximum *ZT* value reached 0.71 at 700 K[19]. Poudel *et al.* fabricated nano-sized bismuth antimony telluride bulk alloys by ball milling and hot pressing method, and the obtained maximum *ZT* value was 1.4 at 373 K[20]. Li *et al.* fabricated $Yb_{0.2}Co_4Sb_{12+y}$ bulk materials with nanostructure by combining melt spinning technique with spark plasma sintering, and the maximum *ZT* value reached 1.26 at 800 K[21]. Li *et al.* also prepared *n*-type skutterudites $In_xCe_yCo_4Sb_{12}$ with in-situ forming nano-sized InSb phase by a melt-quench-anneal-spark plasma sintering method, and the maximum *ZT* value of 1.43 was obtained at 800 K[22]. Lan *et al.* found that small nanosized particles located at the grain boundaries or embedded in larger particles could provide effective phonon scattering centers and thus reduced the phonon thermal conductivity efficiently[23]. Pei *et al.* found that there was an enhancement of *ZT* due to phonon scattering at the interfaces, when PbTe was nanostructured with large nanometer sized Ag_2Te precipitates[24]. Ahn *et al.* prepared *p*-type PbTe-MTe (M = Cd, Hg) and found that meso-scale grain boundaries along with nanostructured precipitates play an important role in significantly reducing the lattice thermal conductivity[25]. Above-mentioned studies on thermoelectric materials with nanocomposite gave us some good inspirations.

Herein, we reported an effective path to enhance the thermoelectric performance of *n*-type oxide, Nb-doped $SrTiO_3$ ($SrNb_{0.15}Ti_{0.85}O_3$, Nb-STO), by yttria stabilized zirconia (YSZ) nano-inclusion with the low thermal conductivity. Our results show the *ZT* value of Nb-STO was enhanced 9-fold, due to the decreased thermal conductivity and meanwhile the increased electrical conductivity, pointing to a robust approach for high-performance *n*-type thermoelectric oxide.

Results

Fig. 1 showed the temperature dependent thermal and electric transport properties of YSZ/Nb-STO composite, namely, the thermal conductivity (κ), electrical conductivity (σ), and Seebeck coefficient (S). Significantly, YSZ inclusion reduced the thermal conductivity (Fig. 1(a)), and meanwhile increased the electrical conductivity (Fig. 1(b). However, Seebeck coefficients were subjected to a very small impact by YSZ inclusion (Fig. 1(c)). The thermal conductivity and the electrical conductivity at 900 K were reduced ~15% and increased 10-fold, respectively.

Fig. 2 showed the temperature dependent electrical conductivity and thermal conductivity of pure YSZ bulk ceramic, with the relative density of 91.6%, prepared by the conventional normal pressure sintering method at 1500°C for 3 h in an Ar atmosphere. The thermal conductivity and the electrical conductivity of YSZ bulk were much lower than those of pure Nb-STO ceramic showed in Fig. 1(a) and Fig. 1(b).

The thermoelectric power factor $S^2\sigma$ and dimensionless figure of merit *ZT* of the composite were shown in Fig. 3. The power factor was increased more than 7-fold as compared with the sample without YSZ inclusion (Fig. 3(a)), which is mainly beneficial from the increased electrical conductivity. Owing to the low thermal conductivity and high electrical conductivity, the *ZT* value is enhanced 9-fold, up to 0.21 at 900 K.

Discussion

The carrier concentration (n), Hall mobility (μ), carrier effective mass (m^*/m_0) and $m^*/n^{2/3}$ at room temperature were summarized in the Table 1. With YSZ inclusion, the mobility was enhanced significantly, however, relatively, there was little change in the carrier concentration, which contributed to the enhancement of the electrical conductivity, according to the relation formula:

$$\sigma = ne\mu. \tag{1}$$

For degenerate semiconductors (parabolic band, energy-independent scattering approximation), the Seebeck coefficient (S) is given by[26]:

$$S = \left(8\pi^2 k_B^2 / 3eh^2\right) m^* T (\pi/3n)^{2/3}, \tag{2}$$

where k_B is Boltzmann constant and h is Planck constant. The equation indicates the Seebeck coefficient strongly depends on the value, $m^*/n^{2/3}$. Table 1 exhibited YSZ inclusion had very small impact on the value, $m^*/n^{2/3}$, which led to that Seebeck coefficient was almost independent of YSZ inclusion.

Temperature dependent electronic thermal conductivity (κ_e), lattice thermal conductivity (κ_L) and phonon mean free path (L_{phonon}) of YSZ/Nb-STO composites were shown in Fig. 4. The κ_e was subtracted from the total thermal conductivity by using the Wiedemann-Franz law:

$$\kappa_e = LT\sigma, \tag{3}$$

where L is the Lorenz factor, 2.45×10^{-8} V^2/K^2. The resulting κ_L was obtained by the relation:

$$\kappa_e = \kappa - \kappa_L. \tag{4}$$

L_{phonon} was evaluated by the following equations[27,28],

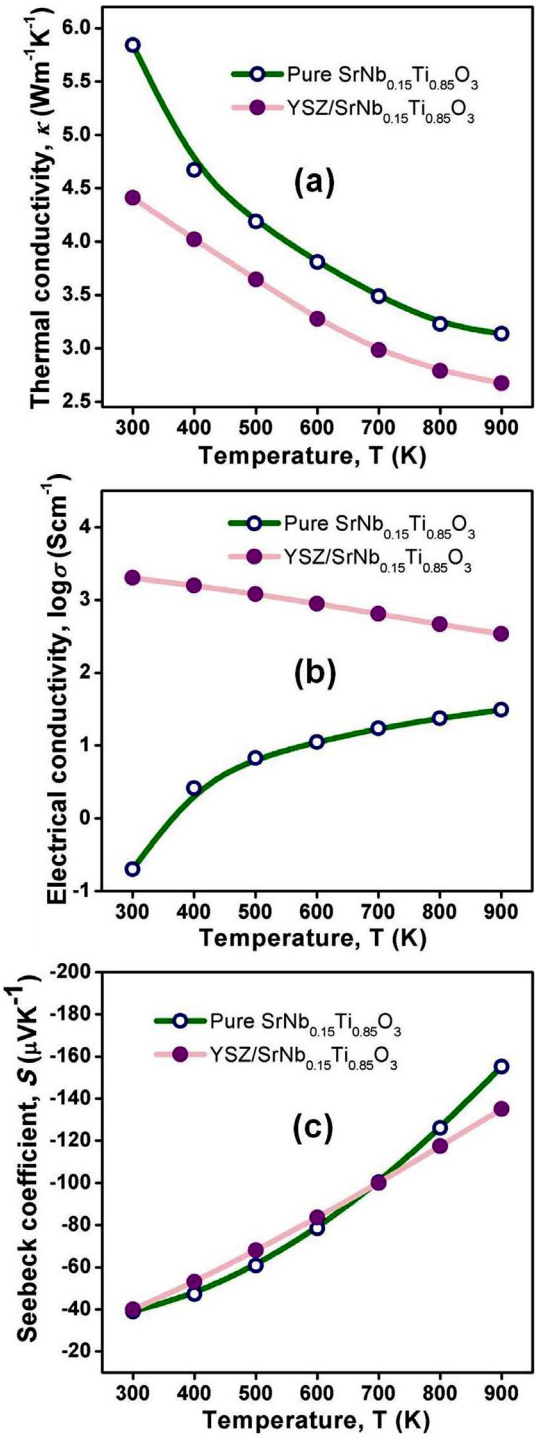

Figure 1 | Temperature dependent thermal and electric transport properties of YSZ/Nb-STO composite. (a) thermal conductivity (κ), (b) electrical conductivity (σ), and (*c*) Seebeck coefficient (S).

$$L_{phonon} = 3\kappa_L \Big/ \left[3^{1/3} C \left(1/V_L^3 + 2/V_S^3\right)^{-1/3}\right], \tag{5}$$

where V_L, V_s, C, were the longitudinal sound velocity, transverse sound velocity and specific heat capacity, respectively. Fig. 4(c) revealed that YSZ inclusion significantly decreased L_{phonon} and further induced the reduction in κ_L (Fig. 4(b)).

Scanning electron micrographs (SEM) of YSZ/Nb-STO composite (Fig. 5(a) and (b)) showed the grain size was increased obviously by YSZ inclusion. To confirm where YSZ existed in bulk Nb-STO

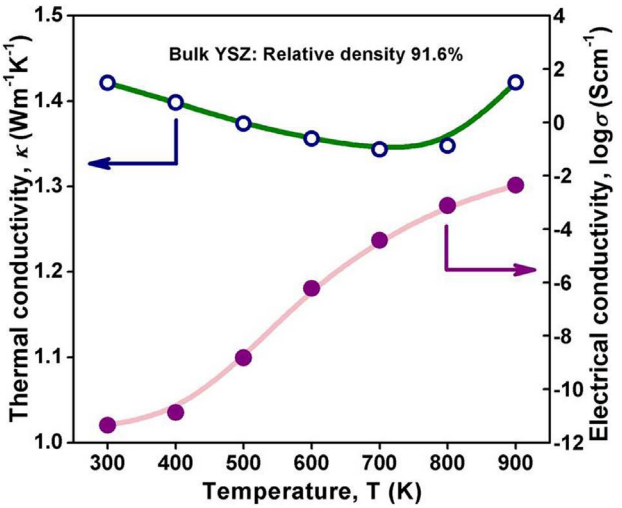

Figure 2 | Temperature dependent electrical conductivity and thermal conductivity of pure YSZ bulk ceramic.

ceramic, transmission electron microscope (TEM) observation and selected area electron diffractions (SAED) were carried out. The SAED patterns in Fig. 5(c-ii) and Fig. 5(d-ii), taken from large crystalline area in Fig. 5(c) and Fig. 5(d), were only well-matched with a cubic strontium titanate crystal. However, the SAED patterns in

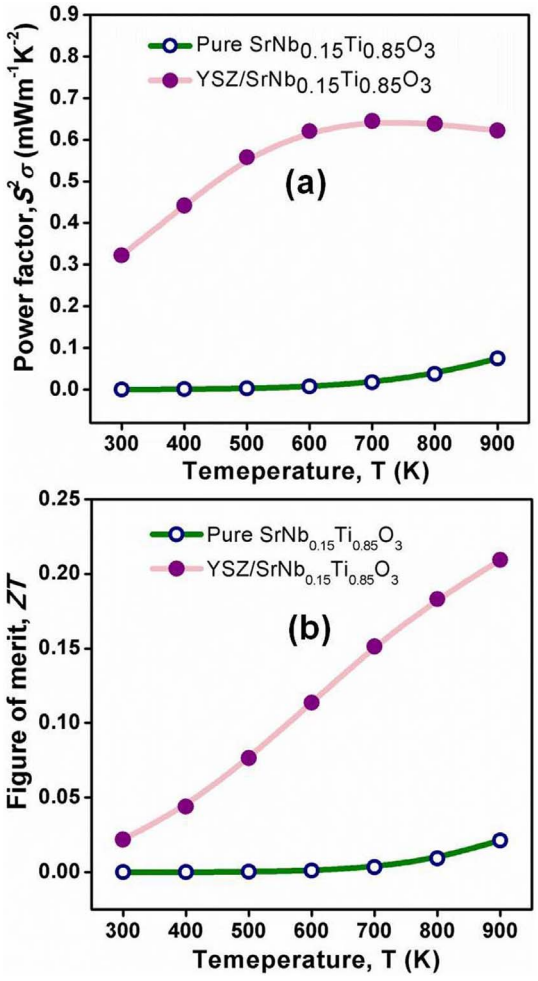

Figure 3 | Temperature dependent thermoelectric power factor $S^2\sigma$ (a) and dimensionless figure of merit ZT (b) of YSZ/Nb-STO composite.

Table 1 | Carrier concentration (n), Hall mobility (μ), carrier effective mass (m^*/m_0, m_0 = free electron mass) and $m^*/n^{2/3}$ at room temperature

	n (10^{21} cm^{-3})	μ (cm^{2}V^{-1}s^{-1})	m^*/m_0	$m^*/n^{2/3}$ (10^{-14} cm^2)
Pure Nb-STO	1.57[†]	8×10^{-4}	1.75	1.29m_0
YSZ/Nb-STO	2.06	6.11	2.16	1.27m_0

[†]estimated using the lattice constant and relative density (63.1%) of pure Nb-STO.

Fig. 5(c-i) and Fig. 5(d-i), taken from black nano-sized particles in Fig. 5(c) and Fig. 5(d), revealed some diffraction spots except the diffraction spots of strontium titanate, which matched the diffraction spots of YSZ very well. Above-mentioned evidences fully proved that YSZ inclusions located inside the grain (Fig. 5 (c)) and in the triple junction (Fig. 5(d)), and these inclusions were nano-sized, from several tens nanometers to several hundreds nanometers. YSZ has much lower thermal conductivity, ~2.5 $Wm^{-1}K^{-1}$ below 1200 K[29], compared with $SrTiO_3$[30].YSZ nano-inclusions inside the grain and in the triple junction could scatter the phonons effectively and thus brought about the decrease in the phonon mean free path, the lattice thermal conductivity and the total thermal conductivity, in sequence. As for $SrTiO_3$ ceramic with oxide additives, such as TiO_2, Al_2O_3 and SiO_2, at the sintering temperature of over than 1400°C, the liquid phase formed at triple grain junctions and exhibited complete wetting of the grain boundaries[31]. YSZ/Nb-STO sample exhibited the abnormal grain growth in our experiment, which could be a similar liquid phase sintering behavior to $SrTiO_3$ ceramic with added TiO_2, Al_2O_3 and SiO_2 in Ref. 31. According to the liquid-phase sintering theory proposed by Kingery[32], the liquid phase formation could lead

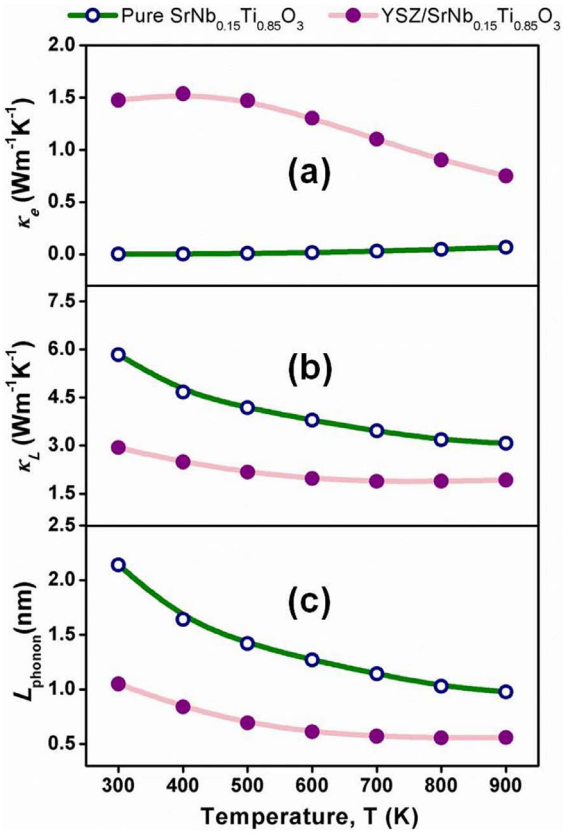

Figure 4 | Temperature dependent electronic thermal conductivity (κ_e) (a), lattice thermal conductivity (κ_L) (b) and phonon mean free path (L_{phonon}) (c) of YSZ/Nb-STO composite.

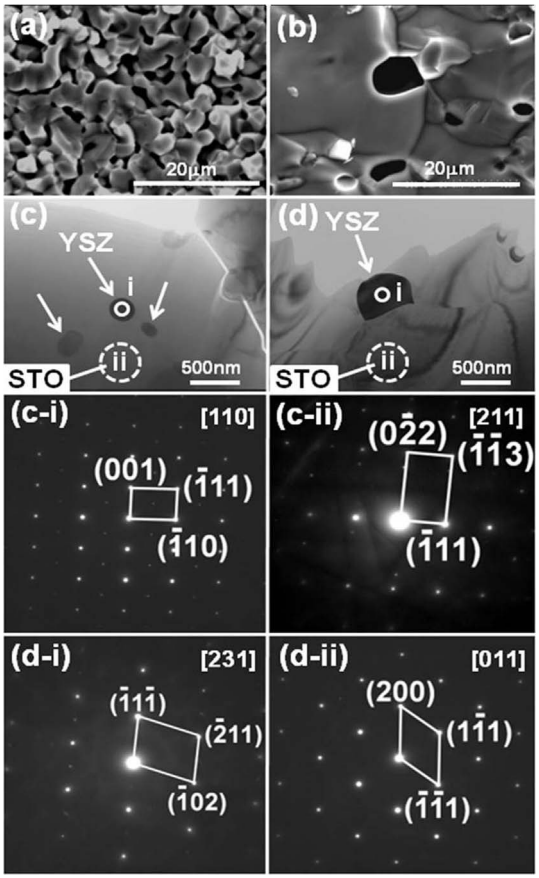

Figure 5 | Microstructures and SAED patterns of YSZ/Nb-STO composite. (a) SEM of sample without YSZ inclusion; (b) SEM of sample with YSZ inclusion; (c) TEM of sample with YSZ inclusion inside grain; (d) TEM of sample with YSZ inclusion in triple junction; (c-i) SAED pattern taken from i-area in Fig. 5(c); (c-ii) SAED pattern taken from ii-area in Fig. 5(c); (d-i) SAED pattern taken from i-area in Fig. 5(d); (d-ii) SAED pattern taken from ii-area in Fig. 5(d).

to the complete wetting of the grain boundaries, increase the grain boundary mobility and thus markedly accelerate the sintering rate and grain growth. The abnormal crystal growth of strontium titanate grain could obviously diminish the number density of grain boundaries and further reduce interface scattering of electrons remarkably, which partly contributed to the increased mobility and further to the enhanced electrical conductivity. On the other hand, Compared with pure Nb-STO, the relative density of YSZ/Nb-STO composite was increased from 63.1% to 79.4%, which was also partly contributed to the enhanced electrical conductivity. Fig. 6 showed the interaction schematic of phonon-nanoinclusion and electron-nanoinclusion. Oxide nano-inclusion with the low thermal conductivity, located inside the grain and in the triple junction, can reduce the thermal conductivity by effective interface phonon scattering, enhance the electrical conductivity by promoting the abnormal grain growth and increasing the relative density, and thus lead to the obvious enhancement of *ZT* value of Nb-STO.

In summary, YSZ nano-inclusion could effectively reduce the thermal conductivity and increase the electrical conductivity of Nb-STO, and thus obviously enhance the *ZT* value, which strongly suggested that oxide nano-inclusion with low thermal conductivity could be an effective strategy to enhance the thermoelectric properties of oxide thermoelectric materials with high thermal conductivity. Oxide nano-inclusion distributed inside the grain and in the triple junction can obviously reduce the phonon mean free path by the effective interface phonon scattering, and further apparently lead

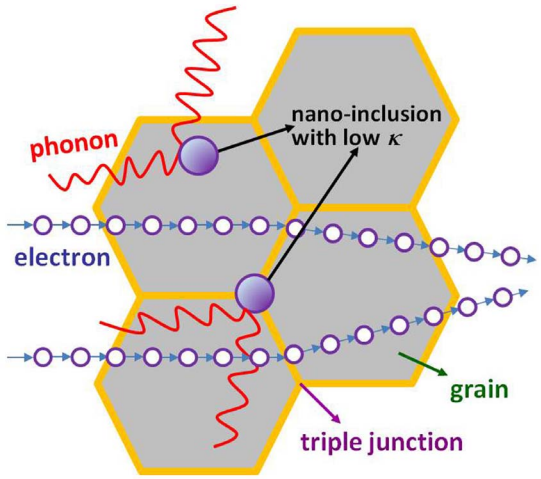

Figure 6 | Schematic of phonon-nanoinclusion interaction and electron-nanoinclusion interaction.

to the decrease in the thermal conductivity. Meanwhile, the oxide nano-inclusion with high surface activation can promote the grain growth, diminish the number density of grain boundaries, increase relative density and thus improve the carrier mobility and the electrical conductivity. Our research may give some helpful enlightenment to develop high-performance oxide thermoelectric materials.

Methods

Sample preparation. Commercial YSZ (8 mol% yttria-stabilized zirconia) particles with the size of 25 ~ 30 nm were used as an oxide inclusion. Nb-doped $SrTiO_3$ ceramic sample with YSZ inclusion of 3 wt% were fabricated by the conventional normal pressure sintering method at 1500°C for 3 h in an Ar atmosphere. The relative densities of Nb-doped $SrTiO_3$ ceramic without added YSZ and with YSZ inclusion of 3 wt% are 63.1% and 79.4%, respectively.

Sample characterization. The thermoelectric performances, such as the Seebeck coefficient and electrical conductivity, were measured at 300–900 K in an Ar atmosphere by using an automatic thermoelectric measuring apparatus (Ozawa RZ2001K). The thermal diffusivity was measured by the usual laser flash method (ULVAC-RIKO TC-9000V). The carrier concentration and mobility was measured by the Van der Pauw's method (RESITEST 8300).The microstructures were observed on a scanning electron microscope (SEM) and a JEM-2010 transmission electron microscope (TEM). The specific heat capacity was measured by a differential scanning calorimeter system (TA Instrument DSC-2910). The mean phonon velocity was measured by an ultrasonic pulse-echo method (Panametrics-NDT 5800). The electrical properties (electrical conductivity and Seebeck coefficient) and thermal conductivity were measured in in-plane and cross-plane directions. YSZ/Nb-STO polycrystalline ceramic composite exhibited the isotropic electrical conductivity, Seebeck coefficient and thermal conductivity.

1. Zebarjadi, M. *et al.* Perspectives on thermoelectrics: from fundamentals to device applications. *Energy Environ. Sci.* **5**, 5147–5162 (2012).
2. Heremans, J. P., Wiendlocha, B. & Chamoire, S. M. Resonant levels in bulk thermoelectric semiconductors. *Energy Environ. Sci.* **5**, 5510–5530 (2012).
3. Biswas, K. *et al.* High-performance bulk thermoelectrics with all-scale hierarchical architectures. *Nature* **489**, 414–418 (2012).
4. Snyder, J. G. & Toberer, E. S. Complex thermoelectric materials. *Nat. Mater.* **7**, 105–114 (2008).
5. Poudel, B. *et al.* High-thermoelectric performance of nanostructured bismuth antimony telluride bulk alloys. *Science* **320**, 634–638 (2008).
6. Li, F. *et al.* Polycrystalline BiCuSeO oxide as a potential thermoelectric material. *Energy Environ. Sci.* **5**, 7188–7195 (2012).
7. Li, J. *et al.* A high thermoelectric figure of merit ZT > 1 in Ba heavily doped BiCuSeO oxyselenides. *Energy Environ. Sci.* **5**, 8543–8547 (2012).
8. Lan, J. L. *et al.* Doping for higher thermoelectric properties in *p*-type BiCuSeO oxyselenide. *Appl. Phys. Lett.* **102**, 123905–123908 (2013).
9. Liu, Y. *et al.* Remarkable enhancement in thermoelectric performance of BiCuSeO by Cu deficiencies. *J. Am. Chem. Soc.* **133**, 20112–20115 (2011).
10. Wang, Y. *et al.* High temperature thermoelectric response of electron-doped $CaMnO_3$. *Chem. Mater.* **21**, 4653–4660 (2009).
11. Inoue, Y., Okamoto, Y. & Morimoto, J. Thermoelectric properties of porous zinc oxide ceramics doped with praseodymium. *J. Mater. Sci.* **43**, 368–377 (2008).

12. Peleckis, G., Motohashi, T., Karppinen, M. & Yamauchi, H. Enhanced thermoelectric properties of $NaxCoO_2$ whisker crystals. *Appl. Phys. Lett.* **83**, 5416–5418 (2003).
13. Ohta, H. *et al.* Giant thermoelectric Seebeck coefficient of a two-dimensional electron gas in $SrTiO_3$. *Nature Mater.* **6**, 129–134 (2007).
14. Ohta, S. *et al.* Large thermoelectric performance of heavily Nb-doped $SrTiO_3$ epitaxial film at high temperature. *Appl. Phys. Lett.* **87**, 092108–092110 (2005).
15. Sui, J. *et al.* Texturation boosts the thermoelectric performance of BiCuSeO oxyselenides. *Energy Environ. Sci.* **6**, 2916–2920 (2013).
16. Ohta, S., Ohta, H. & Koumoto, K. Grain size dependence of thermoelectric performance of Nb-doped $SrTiO_3$ polycrystals. *J. Ceram. Soc. Japan* **114**, 102–105 (2006).
17. Dresselhaus, M. S. *et al.* New directions for low-dimensional thermoelectric materials. *Adv. Mater.* **19**, 1043–1053 (2007).
18. Tang, X. F. *et al.* Preparation and thermoelectric transport properties of high-performance *p*-type Bi_2Te_3 with layered nanostructure. *Appl. Phys. Lett.* **90**, 012102–012104 (2007).
19. Mi, J. L., Zhao, X. B., Zhu, T. J. & Tu, J. P. Improved thermoelectric figure of merit in *n*-type $CoSb_3$ based nanocomposites. *Appl. Phys. Lett.* **91**, 172116–172118 (2007).
20. Poudel, B. *et al.* High-thermoelectric performance of nanostructured bismuth antimony telluride bulk alloys. *Science* **320**, 634–638 (2008).
21. Li, H., Tang, X., Su, X. & Zhang, Q. Preparation and thermoelectric properties of high-performance Sb additional $Yb_{0.2}Co_4Sb_{12+y}$ bulk materials with nanostructure. *Appl. Phys. Lett.* **92**, 202114–202116 (2008).
22. Li, H., Tang, X., Zhang, Q. & Uher, C. High performance $In_xCe_yCo_4Sb_{12}$ thermoelectric materials with in situ forming nanostructured InSb phase. *Appl. Phys. Lett.* **94**, 102114–102116 (2009).
23. Lan, Y. *et al.* Structure study of bulk nanograined thermoelectric bismuth antimony telluride. *Nano lett.* **9**, 1419–1422 (2009).
24. Pei, Y. Z., Heinz, N. A., LaLonde, A. & Snyder, G. J. Combination of large nanostructures and complex band structure for high performance thermoelectric lead telluride. *Energy Environ. Sci.* **4**, 3640–3645 (2011).
25. Ahn, K. *et al.* Enhanced thermoelectric properties of *p*-type nanostructured PbTe–MTe (M = Cd, Hg) materials. *Energy Environ. Sci.* **6**, 1529–1537 (2013).
26. Cutler, M., Leavy, J. F. & Fitzpatrick, R. L. Electronic transport in semimetallic cerium sulfide. *Phys. Rev.* **133**, A1143–A1152 (1964).
27. Clarke, D. R. Materials selection guidelines for low thermal conductivity thermal barrier coatings. *Surf. Coat. Technol.* **163**, 67–74 (2003).
28. Kawaharada, Y., Kurosaki, K., Uno, M. & Yamanaka, S. Thermoelectric properties of $CoSb_3$. *J. Alloys Compd.* **315**, 193–197 (2001).
29. Winter, M. R. & Clarke, D. R. Thermal conductivity of yttria-stabilized zirconia–hafnia solid solutions. *Acta Mater.* **54**, 5051–5059 (2006).
30. Suemune, Y. Thermal conductivity of $BaTiO_3$ and $SrTiO_3$ from 4.5° to 300°K. *J. Phys. Soc. Jpn.* **20**, 174–175 (1965).
31. Fujimoto, M. & KINGERY, W. D. Microstructures of $SrTiO_3$ internal boundary layer capacitors during and after processing and resultant electrical properties. *J. Am. Ceram. Soc.* **68**, 169–173 (1985).
32. Kingery, W. D. & Narasimhan, M. D. Densification during sintering in the presence of a liquid phase. *J. Appl. Phys.* **30**, 307–310 (1959).

Acknowledgments

This work was partially supported by China-Japan International Cooperation Program Funds (No. 2010DFA61410 and 2011DFA50530), National Natural Science Foundations of China (No. 51272037, 51272035 and 51362026), Fundamental Research Funds for the Central Universities (No. ZYGX2010Z003), and Program for New Century Excellent Talents in University (No. NCET-12-0097).

Author contributions

N.W. and K.K. designed the experiments. N.W. carried out the fabrication of materials and thermoelectric measurements. W.N. and M.K. contributed to microstructural characterizations. H.J.C. and H.C.H. provided helps in the experiments. N.W. and H.J.C. wrote the paper, and all authors reviewed the manuscript.

Additional information

Competing financial interests: The authors declare no competing financial interests.

How to cite this article: Wang, N. *et al.* Enhanced thermoelectric performance of Nb-doped $SrTiO_3$ by nano-inclusion with low thermal conductivity. *Sci. Rep.* **3**, 3449; DOI:10.1038/srep03449 (2013).